On the Power of Manifold Samples in Exploring Configuration Spaces
and the Dimensionality of Narrow Passages*

Oren Salzman, Michael Hemmer, and Dan Halperin

Abstract We extend our study of Motion Planning via Manifold Samples (MMS), a general algorithmic framework that combines geometric methods for the exact and complete analysis of low-dimensional configuration spaces with sampling-based approaches that are appropriate for higher dimensions. The framework explores the configuration space by taking samples that are *entire low-dimensional manifolds of the configuration space* capturing its connectivity much better than isolated point samples. The contributions of this paper are as follows: (i) We present a recursive application of MMS in a six-dimensional configuration space, enabling the coordination of two polygonal robots translating and rotating amidst polygonal obstacles. In the adduced experiments for the more demanding test cases MMS clearly outperforms PRM, with over 20-fold speedup in a *coordination-tight* setting. (ii) A probabilistic completeness proof for the most prevalent case, namely MMS with samples that are affine subspaces. (iii) A closer examination of the test cases reveals that MMS has, in comparison to standard sampling-based algorithms, a significant advantage in scenarios containing *high-dimensional narrow passages*. This provokes a novel characterization of narrow passages which attempts to capture their dimensionality, an attribute that had been (to a large extent) unattended in previous definitions.

Oren Salzman
Tel-Aviv University, Tel Aviv 69978. ISRAEL, e-mail: orenzalz@post.tau.ac.il

Michael Hemmer
Tel-Aviv University, Tel Aviv 69978. ISRAEL, e-mail: mhsaar@googlemail.com

Dan Halperin
Tel-Aviv University, Tel Aviv 69978. ISRAEL, e-mail: danha@post.tau.ac.il

* This work has been supported in part by the 7th Framework Programme for Research of the European Commission, under FET-Open grant number 255827 (CGL—Computational Geometry Learning), by the Israel Science Foundation (grant no. 1102/11), and by the Hermann Minkowski–Minerva Center for Geometry at Tel Aviv University.

1 Introduction

Configuration spaces, or C-spaces, are fundamental tools for studying a large variety of systems. A point in a d-dimensional C-space describes one state (or configuration) of a system governed by d parameters. C-spaces appear in diverse domains such as graphical animation, surgical planning, computational biology and computer games. For a general overview of the subject and its applications see [8, 22, 24]. The most typical and prevalent example are C-spaces describing mobile systems ("robots") with d degrees of freedom (*dof*s) moving in some *workspace* amongst obstacles. As every point in the configuration space $\mathcal{C}$ corresponds to a *free* or *forbidden* pose of the robot, $\mathcal{C}$ decomposes into disjoint sets $\mathcal{C}_{\text{free}}$ and $\mathcal{C}_{\text{forb}}$, respectively. Thus, the motion-planning problem is commonly reduced to the problem of finding a path that is fully contained within $\mathcal{C}_{\text{free}}$.

1.1 Background

C-spaces haven been intensively studied for over three decades. Fundamentally, two major approaches exist:
(i) Analytic solutions: The theoretical foundations, such as the introduction of C-spaces [26] and the understanding that constructing a C-space is computationally hard with respect to the number of *dofs* [28], were already laid in the late 1970's and early 1980's in the context of motion planing. Exact analytic solutions to the general motion planning problem as well as for various low-dimensional instances have been proposed in [3, 6, 7, 31] and [1, 2, 14, 26, 30], respectively. For a survey of related approaches see [32]. However, only recent advances in applied aspects of computational geometry made robust implementations for important building blocks available. For instance, Minkowski sums, which allow the representation of the C-space of a translating robot, have robust and exact two- and three-dimensional implementations [12, 13, 35]. Likewise, implementations of planar arrangements[2] for curves [34, C.30], could be used as essential components in [31].
(ii) Sampling-based approaches: Sampling-based approaches, such as Probabilistic Roadmaps (PRM) [19], Expansive Space Trees (EST) [16] and Rapidly-exploring Random Trees (RRT) [23], as well as their many variants, aim to capture the connectivity of $\mathcal{C}_{\text{free}}$ in a graph data structure, via random sampling of configurations. For a general survey on the field see [8, 24]. As opposed to analytic solutions these approaches are also applicable to problems with a large number of *dof*. Importantly, the PRM and RRT algorithms were shown to be probabilistically complete [17, 20, 21], that is, they are guaranteed to find a valid solution, if one exists. However, the required running time for finding such a solution cannot be computed for new queries at run-time. This is especially problematic as these algorithms suffer from high sensitivity

[2] A subdivision of the plane into zero-dimensional, one-dimensional and two-dimensional cells, called vertices, edges and faces, respectively induced by the curves.

to the so-called "narrow passage" problem, e.g., where the robot is required to move in environments cluttered with obstacles, having low clearance.

Though there are also some hybrid approaches [10, 15, 25, 36] it is apparent that the arsenal of currently available motion-planning algorithms lacks a general scheme applicable to high-dimensional problems with little or low sensitivity to narrow passages. In [29] we introduced a framework for Motion Planning via Manifold Samples (MMS), which should also be considered as a hybrid approach. In a setting considering a three-dimensional C-space it was capable of achieving twenty-fold (and more) speedup factor in running time when compared to the PRM algorithm when used for planning paths within narrow passages. We believe that the speedup presented in [29] does not present a mere algorithmic advantage for a specific implemented instance but a fundamental advantage of the framework when solving scenarios with narrow passages.

This study attempts to continue developing the MMS framework as a tool to overcome the gap mentioned in existing motion-planning algorithms. We briefly present the scheme and continue to a preliminary discussion on applying MMS in high-dimensional C-spaces, which motivates this paper.

1.2 Motion Planning via Manifold Samples

The framework is presented as a means to explore the *entire* C-space, or, in motion-planning terminology as a multi-query planner, consisting of a preprocessing stage and a query stage. The preprocessing stage constructs the *connectivity graph* $\mathcal{G}$ of $\mathcal{C}$, a data structure that captures the connectivity of $\mathcal{C}$ using *entire low-dimensional manifolds* as samples. The manifolds are decomposed into cells in $\mathcal{C}_{\text{free}}$ and $\mathcal{C}_{\text{forb}}$ in an analytic manner; we call a cell of the decomposed manifold that lies in $\mathcal{C}_{\text{free}}$ a *free space cell* (FSC). The FSCs serve as nodes in $\mathcal{G}$. Two nodes in are connected by an edge if their corresponding FSCs intersect. See Fig. 1 for an illustration.

Once $\mathcal{G}$ has been constructed it can be queried for paths between two configurations $q_s, q_t \in \mathcal{C}_{\text{free}}$ in the following manner: A manifold that contains q_s in one of its FSCs is generated and decomposed (similarly for q_t). These FSCs and their appropriate edges are added to $\mathcal{G}$. We compute a path γ in $\mathcal{G}$ between the FSCs that contain q_s and q_t. If such a path in $\mathcal{G}$ is found, it can be (rather straightforwardly) transformed into a continuous path in $\mathcal{C}_{\text{free}}$ by planning a path within each FSC in γ.

1.3 MMS in Higher Dimensions

The successful application of MMS in [29] to a three-dimensional C-space can be misleading when we come to apply it to higher dimensions. The heart of the scheme is the choice of manifolds from which we sample. Informally, for the scheme to work we must require that the used set of manifolds $\mathcal{M}$ fulfills the following conditions.

C1 The manifolds in $\mathcal{M}$ cover the C-space.

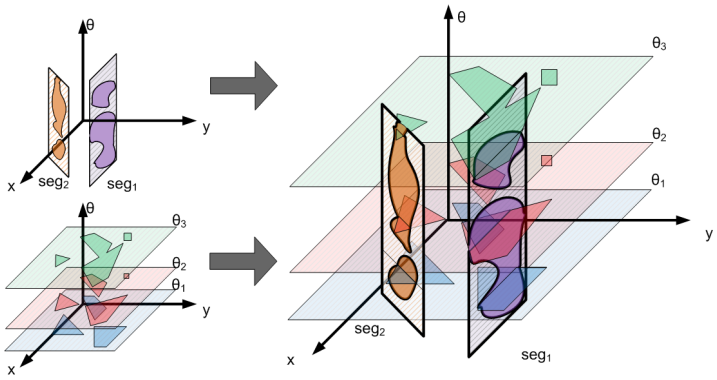

Fig. 1: Three-dimensional C-spaces: The left side illustrates two families of manifolds where the decomposed cells are darkly shaded. The right side illustrates their intersection that induces the graph $\mathcal{G}$. Figure taken from [29].

C2 A pair of surfaces chosen uniformly and independently[3] at random from $\mathcal{M}$ intersect with significant probability.
C3 Manifolds need to be of very low dimension as MMS requires an analytic description of the C-space when restricted to a manifold. Otherwise the machinery for a construction of this description is not readily available.

For MMS to work in C-spaces of dimension d, Condition **C2** has a prerequisite that the sum of dimensions of a pair of manifolds chosen uniformly and independently at random from $\mathcal{M}$ is at least d with significant probability. This means in particular that $\mathcal{M}$ will consist of manifolds of dimension[4] $\lceil \frac{d}{2} \rceil$. With this prerequisite in mind, there is already what to gain from using our existing and strong machinery for analyzing two-dimensional manifolds [4, 5, 11], while fulfilling the conditions above: We can solve motion-planning problems with four degrees of freedom, at the strength level that MMS offers, which is higher than that of standard sampling-based tools.

However, we wish to advance to higher-dimensional C-spaces in which satisfying all the above conditions at once is in general impossible. We next discuss two possible relaxations of the conditions above that can lead to effective extensions of MMS to higher dimensions.

Dependent choice of manifolds: If we insist on using only very low-dimensional manifolds even in higher-dimensional C-spaces, then to guarantee that pairs of manifolds intersect, we need to impose some dependence between the choices of manifolds, i.e., relaxing condition **C2**. A natural way to impose intersections between manifolds is to adapt the framework of tree-

[3] The requirement that the choices are independent stems from the way we prove completeness of the method. It is not necessarily an essential component of the method itself.

[4] The precise statement is somewhat more involved and does not contribute much to the informal discussion here. Roughly, $\mathcal{M}$ should comprise manifolds of dimension $\lceil \frac{d}{2} \rceil$ or higher and possibly manifolds of their co-dimension.

based planners like RRT [23]. When we add a new manifold, we insist that it connects either directly or by a sequence of manifolds to the set of manifolds collected in the data structure (tree in the case of RRT) so far.

Approximating manifolds of high dimension: As we do not have the machinery to exactly analyze C-spaces restricted to manifolds of dimension three or higher, we suggest to substitute exact decomposition of the manifolds as induced by the C-space by some approximation. i.e., relaxing condition **C3**. There are various ways to carefully approximate C-spaces. In the rest of the paper we take the approach of *a recursive application of MMS*.

In Section 2 we demonstrate this recursive application for a specific problem in a six-dimensional configuration space, namely the coordination of two planar polygonal robots translating and rotating admits polygonal obstacles. In the adduced experiments for the more demanding test cases MMS clearly outperforms PRM, with over 20-fold speedup in an especially tight setting. Section 3 provides the theoretical foundations for using MMS in a recursive fashion. In Section 4 we examine the significant advantage of MMS with respect to prevailing sampling-based approaches in scenarios containing *high-dimensional narrow passages*. This provokes a novel characterization of narrow passages which attempts to capture their dimensionality. We conclude with an outlook on further work in Section 5.

2 The Case of Two Rigid Polygonal Robots

We discuss the MMS framework applied to the case of coordinating the motion of two polygonal robots R_a and R_b translating and rotating in the plane amidst polygonal obstacles. Each robot is described by the position of its reference point $r_a, r_b \in \mathbb{R}^2$ and the amount of counter-clockwise rotation $\theta_a, \theta_b \in S^1$ with respect to an initial orientation. All placements of R_a in the workspace $\mathcal{W}$ induce the three-dimensional space $\mathcal{C}^a = \mathbb{R}^2 \times S^1$. Similarly for R_b. We describe the full system by the six-dimensional C-space $\mathcal{C} = \mathcal{C}^a \times \mathcal{C}^b$.

2.1 Recursive Application of the MMS framework

We first assume (falsely) that we have the means to decompose three-dimensional manifolds. Under this assumption, the application of MMS is straightforward: The set $\mathcal{M}$ consists of two families. The first family of manifolds is defined by fixing R_b at free configurations $b \in \mathcal{C}^b_{\text{free}}$ while R_a moves freely inducing the three-dimensional subspaces[5] $\mathcal{C}^a \times b$. The second family is defined symmetrically by fixing R_a. As subspace pairs of the form $(a \times \mathcal{C}^b, \mathcal{C}^a \times b)$ intersect at the point (a, b), manifolds of the two families intersect allowing for connections in the connectivity graph $\mathcal{G}$.

[5] In this paper, when discussing subspaces, we should actually use the term affine subspaces or linear manifolds. We allow ourselves this (slight) inaccuracy for ease of reading.

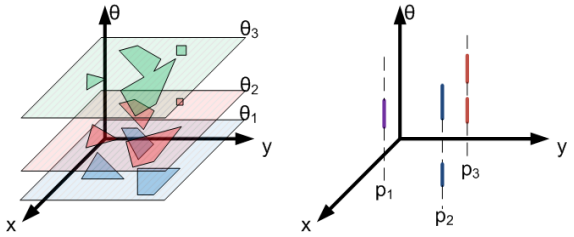

(a) Horizontal slices (b) Vertical lines

Fig. 2: Manifolds families and their FSCs. FSCs of horizontal slices are polygons while FSCs of vertical lines are intervals along the line.

However, we do not have the tools to construct three-dimensional manifolds explicitly. Thus the principal idea is to construct *approximations* of these manifolds by another application of MMS. Since for a certain manifold one robot is fixed, we are left with a three-dimensional C-space in which the fixed robot is regarded as an obstacle. Essentially this is done by using the implementation presented in [29] but with a simpler set of manifolds (see also Fig. 2): (i) **Horizontal slices** – corresponding to a fixed orientation of the moving robot while it is free to translate (ii) **Vertical lines** – corresponding to a fixed location of the moving robot while it is free to rotate.

This recursive application of MMS is not straightforward since it must be ensured that the approximations of the three-dimensional subspaces intersect. We overcome this difficulty by randomly sampling a set Θ_a and Θ_b of angles for the two robots. When constructing a subspace for moving robot R_a, we construct a horizontal slice for each angle in Θ_a. When fixing robot R_a, we sample its orientation from the set Θ_a. Similar for robot R_b. This way, pairs of approximated subspaces are bound to intersect.

2.2 Implementation Details

Horizontal slices: Let R_m and R_f denote the moving and fixed robot, respectively. Θ_m denotes the set of angles that is sampled for R_m upfront. A horizontal plane for an angle $\theta_m \in \Theta_m$ is defined by the Minkowski sum of $-R_{\theta_m}$with all obstacles and, in addition, with the fixed robot.[6] However, for each approximation of a three-dimensional affine subspace of robot R_m we are using the same set of angles, namely Θ_m. Only the position of robot R_f changes. Therefore, for all $\theta_m \in \Theta_m$ we precompute the Minkowski sum of robot $-R_{\theta_m}$ with all obstacles. In order to obtain a concrete slice we only add the Minkowski sum of $-R_{\theta_m}$ with R_f by a simple overlay.

Vertical lines: Limiting the movement of R_m to rotating about a fixed point results in a vertical line in the three-dimensional C-space. Each vertex (or edge) of the robot in combination with each edge (or vertex) of an obstacle (or the fixed robot) gives rise to up to two critical angles on this line. These

[6] $-R_{\theta_m}$ denotes R_m rotated by θ_m and reflected about the origin.

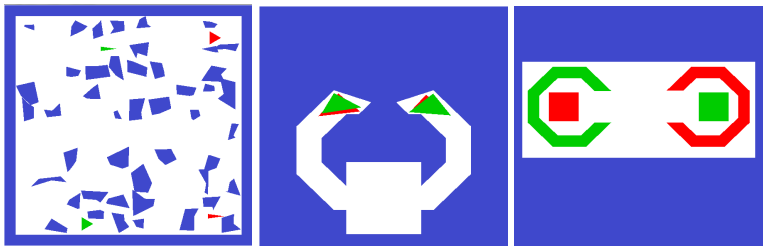

(a) Random polygons (b) Viking helmet (c) Pacman

Fig. 3: Experimental scenarios

critical values mark a potential transition between $\mathcal{C}_{\text{forb}}$ and $\mathcal{C}_{\text{free}}$. Thus a vertical line is constructed by computing these critical angles and the FSCs are maximal free intervals along this line (for further details see the Appendix)

2.3 Experimental Results

We demonstrate the performance of our planner using three different scenarios. All scenarios consist of a workspace, obstacles, two robots and one query (source and target configurations). All reported tests were measured on a Dell 1440 with one 2.4GHz P8600 Intel Core 2 Duo CPU processor and 3GB of memory running with a Windows 7 32-bit OS. Preprocessing times presented are times that yielded at least 80% (minimum of 5 runs) success rate in solving queries. The algorithm is implemented in C++ based on CGAL [34], which is used for the geometric primitives, and the BOOST graph library [33], which is used to represent the connectivity graph $\mathcal{G}$.

Fig. 3 illustrates the scenarios where the obstacles are drawn in blue and the source and target configurations are drawn in green and red, respectively. We used an implementation of the PRM algorithm as provided by the OOPSMP package [27]. For fair comparison, we did not use cycles in the roadmap as cycles increase the preprocessing time significantly. We manually optimized the parameters of each planner over a concrete set. The parameters for MMS are: n_θ – the number of sampled angles; n_ℓ – the number of vertical lines; n_f – the number of times some robot is fixed to a certain configuration while the three-dimensional C-space of the other is computed. The parameters used for the PRM are the number of neighbors (denoted k) to which each milestone should be connected and the percentage of time used to sample new milestones (denoted % st). The results are summarized in Table 1.

The Random polygons scenario[7] is an easy scenario where little coordination is required. Both planners require the same amount of time to solve this case. We see that even though our planner uses complex primitives, when

[7] Scenario provided as part of the OOPSMP distribution

Scenario	MMS				PRM			Speedup
	n_θ	n_ℓ	n_f	t	k	% st	t	
Random polygons	5	512	2	8	20	0.025	8	1
Viking helmet	20	16	10	6.2	14	0.0125	40	6.45
Pacman	5	4	180	17.6	20	0.0125	20	3.5

Table 1: Comparison With PRM

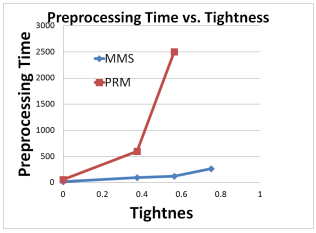

Fig. 4: Tightness Results

using the right parameters, it can handle simple cases with no overhead when compared to the PRM algorithm.

The Viking-helmet scenario consists of two narrow passages that each robot needs to pass through. Moreover, coordination is required for the two robots to exchange places in the lower chamber. We see that the running times of the MMS are favorable when compared to the PRM implementation. Although each robot is required to move along a narrow passage, the motion along this passage does not require coordination, this is not exploited by the PRM algorithm.

The Pacman scenario, in which the two robots need to exchange places, requires coordination of the robots: they are required to move into a position where the C-shaped robot, or pacman, "swallows" the square robot, the pacman is then required to rotate around the robot. Finally the two robots should move apart (see Fig. 5). We ran this scenario several times, progressively increasing the square robot size. This caused a "tightening" of the passages containing the desired path. Fig. 4 demonstrates the preprocessing time as a function of the tightness of the problem for both planners. A tightness of zero denotes the base scenario (Fig. 3c) while a tightness of one denotes the tightest solvable case. Our algorithm has less sensitivity to the tightness of the problem as opposed to the PRM algorithm. In the tightest experiment solved by the PRM, MMS runs 20 times faster. We ran the experiment on a tighter scenario but terminated the PRM algorithm after 5000 seconds. We believe that behavior of the algorithms with respect to the tightness of the passage is a fundamental difference between the two algorithms and discuss its origin in Section 4.

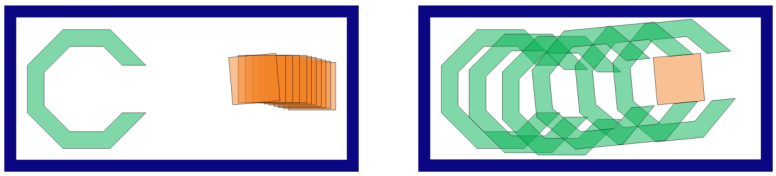

(a) The square robot moves into a position where the pacman can engulf it

(b) The pacman engulfs the square robot

Fig. 5: Example of a path in the Pacman Scenario

3 Probabilistic Completeness of MMS

It has been shown that PRM, using point samples, is probabilistically complete (see, e.g., [8, C.7]). At first glance it may seem that if the scheme is complete for point samples then it is evidently complete when these samples are substituted with manifold samples: manifolds of dimension one or higher guarantee better coverage of the configuration space. However, there is a crucial difference between PRM and MMS when it comes to connectivity. The completeness proof for PRM relies, among others facts, on the fact that if the straight line segment in the configuration space connecting two nearby samples lies in the free space, then the nodes corresponding to these two configurations are connected by an edge in the roadmap graph. The connectivity in MMS is attained through intersections of manifolds, which may require a chain of subpaths on several distinct manifolds to connect two nearby free configurations. This is what makes the completeness proof for MMS non trivial and is expressed in Lemma 3.2 below.

We present a probabilistic completeness proof for the MMS framework for the case where the configuration space $\mathcal{C}$ is the d-dimensional Euclidean space $\mathbb{R}^d$ while MMS is taking samples from two perpendicular affine subspaces, the sum of whose dimension is d. Assuming Euclidean space does not impose a real restriction as long as the actual C-space can be embedded into a Euclidean space. Also in more complex cases such as periodic parameters this only requires some minor technical modifications.

Let A and B denote such subspaces and let k and $d-k$ be their dimensions, respectively. As $\mathcal{C}$ is decomposed into two perpendicular subspaces, a point $p = (a_1, \ldots, a_k, b_1, \ldots, b_{d-k}) \in \mathcal{C}$ may be represented as the pair of points (a, b) from subspaces A and B. Under this assumption, the set of manifolds $\mathcal{M}$ consists of two families of $(d-k)$ and k-dimensional manifolds $\mathcal{M}^A$ and $\mathcal{M}^B$. Family $\mathcal{M}^A$ consists of all manifolds that are defined by fixing a point $a_0 \in A$ while the remaining $d-k$ parameters are variable, $\mathcal{M}^B$ is defined symmetrically. Two manifolds $m(a) \in \mathcal{M}^A$ and $m(b) \in \mathcal{M}^B$ always intersect in exactly one point, i.e., $m(a) \cap m(b) = (a, b) \in \mathcal{C}$. Let $B_r^{\mathcal{C}}(p) = \{q \in \mathcal{C} \mid dist(p, q) \leq r\}$ define a ball in $\mathcal{C}$ of radius r centered at $p \in \mathcal{C}$, where $dist$ denotes the Euclidean metric on $\mathcal{C}$. Likewise, $B_r^B(b)$ and $B_r^A(a)$ denote $d-k$ and k-dimensional balls in B and A, respectively.

Definition 1 (ρ-intersecting). For $\rho > 0$ we term a manifold $m(a) \in \mathcal{M}^A$ ρ-*intersecting* for a point $p \in \mathcal{C}$ if $m(a) \cap B_\rho^{\mathcal{C}}(p) \neq \emptyset$, i.e., if $a \in B_\rho^A(p_A)$, where p_A is the projection of p into A. Similarly for manifolds in B.

A feasible path γ is a continuous mapping from the interval $[0, 1]$ into $\mathcal{C}_{\text{free}}$. The image of a path is defined as $Im(\gamma) = \{\gamma(\alpha) \mid \alpha \in [0, 1]\}$. We show that for any collision-free path $\gamma_{p,q}$ of clearance $\rho > 0$ between two configurations p and q, the probability that MMS constructs a path from p to q with distance at most ρ from $\gamma_{p,q}$ on the union of the sampled manifolds is pos-

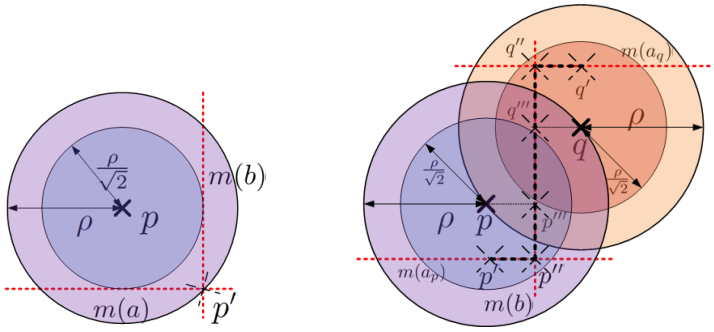

Fig. 6: Two-dimensional sketch: balls and manifolds are presented as circles and lines, respectively. (a) Intersection of two $\rho/\sqrt{2}$-intersecting manifolds. (b)!Construction of a path as defined in Lemma 3.2.

itive. Moreover, the probability of failing to find such a path by the MMS algorithm decreases exponentially with the number of samples.

Lemma 3.1 *For $p \in \mathcal{C}$ and $\rho > 0$ let $m(a) \in \mathcal{M}^A$ and $m(b) \in \mathcal{M}^B$ be two manifolds that are $\rho/\sqrt{2}$-intersecting. Their intersection point $p' = (a, b) = m(a) \cap m(b)$ is in $B^{\mathcal{C}}_{\rho}(p)$.*

Proof. $m(a)$ is $\rho/\sqrt{2}$-intersecting for p. Hence, we know that the distance of a to p_A is less than $\rho/\sqrt{2}$, the same holds for b and p_B. Thus we can conclude (as demonstrated in Fig. 6a):

$$dist(p, p') = \sqrt{dist(p_A, a)^2 + dist(p_B, b)^2} \leq \rho.$$

□

The following lemma shows that for any two points p and q, a manifold $m(b) \in \mathcal{M}^B$ that is close to both points enables a connection between two manifolds $m(a_p), m(a_q) \in \mathcal{M}^A$ that are close to p and q, respectively.

Lemma 3.2 *Let $p, q \in C$ be two points such that $dist(p, q) \leq \rho$ and let $m(a_p), m(a_q) \in \mathcal{M}^A$ be two $\rho/\sqrt{2}$-intersecting manifolds for p and q respectively. Let $m(b) \in \mathcal{M}^B$ be a manifold that is simultaneously $\rho/\sqrt{2}$-intersecting for p and q and let $p' = (a_p, p_B) \in B^{\mathcal{C}}_{\rho}(p)$ and $q' = (a_q, q_B) \in B^{\mathcal{C}}_{\rho}(q)$ be the projection of p and q on $m(a_p)$ and $m(a_q)$, respectively.*

There exists a path $\gamma_{p',q'}$ between p' and q' such that $Im(\gamma_{p',q'}) \subseteq (B^{\mathcal{C}}_{\rho}(p) \cup B^{\mathcal{C}}_{\rho}(q)) \cap (m(a_p) \cup m(b) \cup m(a_q))$, i.e. there is a path lying on the manifolds within the union of the balls.

Proof. Let $p'' = m(a_p) \cap m(b) = (a_p, b)$ and $q'' = m(a_q) \cap m(b) = (a_q, b)$ denote the intersection point of $m(a_p)$ and $m(a_q)$ with $m(b)$, respectively. Moreover, let $p''' = (p_A, b) \in B^{\mathcal{C}}_{\rho}(p)$ and $q''' = (q_A, b) \in B^{\mathcal{C}}_{\rho}(q)$ denote the projections of p and q on $m(b)$. We show that the path composed of the segments

(p', p''), (p'', p'''), (p''', q'''), (q''', q'') and (q'', q') fulfills the requirements. See Fig. 6b.

By Lemma 3.1 the intersection points p'' and q'' are inside $B_\rho^{\mathcal{C}}(p)$ and $B_\rho^{\mathcal{C}}(q)$, respectively. Thus, by convexity of each ball the segments $(p', p'') \subset m(q_p)$ and $(q', q'') \subset m(a_q)$ as well as the segments $(p'', p'''), (q'', q''') \subset m(b)$ are in $(B_\rho^{\mathcal{C}}(p) \cup B_\rho^{\mathcal{C}}(q))$.

It remains to show that $(p''', q''') \subset m(b)$ is inside $(B_\rho^{\mathcal{C}}(p) \cup B_\rho^{\mathcal{C}}(q))$. Recall that $dist(p, q) \leq \rho$ and therefore $dist(p''', q''') \leq \rho$. Let $\bar{p}$ be a point on the segment (p''', q''') that, w.l.o.g, is closer to p'''. Thus $dist(\bar{p}, p''') \leq \rho/2$. The manifold $m(b)$ is $\rho/\sqrt{2}$-intersecting, thus $dist(p, p''') \leq \rho/\sqrt{2}$. As the segments (p, p''') and $(p''', \bar{p})$ are perpendicular it holds:

$$dist(p, \bar{p}) = \sqrt{dist(p, p''')^2 + dist(p''', \bar{p})^2} \leq \sqrt{\rho^2/2 + \rho^2/4} < \rho.$$

□

Theorem 3.3 *Let $p, q \in \mathcal{C}_{\text{free}}$ such that there exists a collision-free path $\gamma_{p,q} \in \Gamma$ of length L and clearance ρ between p and q. Then the probability of the MMS algorithm to return a path between p and q after generating n_A and n_B manifolds from families $\mathcal{M}^A$ and $\mathcal{M}^B$ is:*

$$\begin{aligned} Pr[(p,q)\text{SUCCESS}] &= 1 - Pr[(p,q)\text{FAILURE}] \\ &\geq 1 - \left\lceil \frac{L}{\rho} \right\rceil \left[(1-\mu_A)^{n_A} + (1-\mu_B)^{n_B} \right], \end{aligned}$$

where μ_A and μ_B are some positive constants.

Proof. Let $l = \lceil L/\rho \rceil$, there exists a sequence $[p_0 \dots p_\ell]$ such that $p_i \in Im(\gamma_{p,q})$, $p_0 = p$, $p_\ell = q$, $B_\rho(p_i) \in \mathcal{C}_{\text{free}}$ and $dist(p_i, p_{i+1}) \leq \rho$. MMS adds the manifolds $m(p_A)$ and $m(q_A)$ to the connectivity graph.

Let $A' \subset A$, $|A'| = n_A$ and $B' \subset B$, $|B'| = n_B$, be the two point sets that define the manifolds $M^{A'}$ and $M^{B'}$ that are used by the MMS algorithm. If there is a subset $\{m(a_1) \dots m(a_{\ell-1})\} \subseteq M^{A'}$ and a subset $\{m(b_1) \dots m(b_{\ell-1})\} \subseteq M^{B'}$ such that $(p_i, p_{i+1}, m(a_i), m(b_i), m(a_{i+1}))$ fulfill the conditions of Lemma 3.2 for $i \in \{0 \dots \ell - 1\}$, then there exists a path from p to q in the FSCs constructed by the MMS framework, namely the path which is the concatenation of paths constructed in Lemma 3.2. This implies that p and q are in the same connected component of $\mathcal{G}$, which implies that MMS constructs a path in $\mathcal{C}_{\text{free}}$ from p to q.

Let $I_1 \dots I_{\ell-1}$ be a set of indicator variables such that each I_i witnesses the event that there is a $\rho/\sqrt{2}$-intersecting manifold for p_i in $M^{A'}$. (For p_0 and p_ℓ this is trivially the case due the explicit construction of $m(p_A)$ and $m(q_A)$.) Let $J_0 \dots J_{\ell-1}$ be a set of indicator variables such that each J_i witnesses the event that there is a manifold in $M^{B'}$ that is simultaneously $\rho/\sqrt{2}$-intersecting for p_i and p_{i+1}. It follows that MMS succeeds in answering the query (p, q) if $I_i = 1$ for all $1 \leq i \leq \ell - 1$ and $J_j = 1$ for all $0 \leq j \leq \ell - 1$. Therefore,

$$\begin{aligned} Pr[(p,q)\text{FAILURE}] &\leq Pr\left(\vee_{i=1}^{\ell-1}(I_i=0)\vee_{j=0}^{\ell-1}(J_j=0)\right) \\ &\leq \sum_{i=1}^{\ell-1} Pr[I_i=0] + \sum_{j=0}^{\ell-1} Pr[J_j=0]. \end{aligned}$$

The events $I_i = 0$ and $J_j = 0$ are independent since the samples are taken independent. Thus the probability $Pr[I_i = 0]$, i.e., that not even one of the n_A samples from A is $\rho/\sqrt{2}$-intersecting for p_i is $(1-\mu_A)^{n_A}$, where μ_A is the probability measure that a random sample $a \in A$ defines a manifold that is $\rho/\sqrt{2}$-intersecting for a certain point $p \in \mathcal{C}$. Thus, μ_A is obviously positive. Similarly, $Pr[J_i = 0] = (1-\mu_B)^{n_B}$, where μ_B is the probability measure that a random sample $b \in B$ defines a manifold that is $\rho/\sqrt{2}$-intersecting for a two specific points $p, q \in \mathcal{C}$ with $dist(p,q) < \rho$, that is, it is proportional to the volume of the intersection $B^B_{\rho/\sqrt{2}}(p_B) \cap B^B_{\rho/\sqrt{2}}(q_B)$, which is positive since the radius of the balls is larger than $\rho/2$. Since the sampling is uniform and independent:

$$\begin{aligned} Pr[(p,q)\text{FAILURE}] &\leq \left\lceil \frac{L}{\rho} - 1 \right\rceil (1-\mu_A)^{n_A} + \left\lceil \frac{L}{\rho} \right\rceil (1-\mu_B)^{n_B} \\ &\leq \left\lceil \frac{L}{\rho} \right\rceil \left[(1-\mu_A)^{n_A} + (1-\mu_B)^{n_B}\right]. \end{aligned}$$

□

It follows that as n_A and n_B tend to ∞, the probability of failing to find a path under the conditions stated in Theorem 3.3 tends to zero.

Recursive application The proof of Theorem 3.3 assumes that the samples are taken using full high-dimensional manifolds. However, Section 2 demonstrates a recursive application of MMS where the approximate samples are generated by another application of MMS.

In order to obtain a completeness proof for the two-level scheme let γ be a path of clearance 2ρ. First, assume that the samples taken by the first level of MMS are exact. Applying Theorem 3.3 for γ and ρ shows that with sufficient probability MMS would find a set M' of manifolds that would contain a path γ'. Since we required clearance 2ρ but relied on the tighter clearance ρ, it is guaranteed that γ' still has clearance ρ. Now, each manifold $m' \in \mathcal{M}'$ is actually only an approximation constructed by another application of MMS. Thus, for each $m' \in \mathcal{M}'$ apply Theorem 3.3 to subpath $\gamma'_{m'} = \gamma' \cap m'$ which has clearance ρ. Concatenation of all the resulting subpaths concludes the argument. Of coarse the parameters in the inequality in Theorem 3.3 change accordingly

We remark that the recursive approach imposes a mild restriction on the sampling scheme as the sampling and the approximation must be somewhat coordinated. Since in theory $m(a) \cap m(b) = (a,b)$ we must ensure that points that we sample from A are contained in every approximation of $m(b) \in \mathcal{M}^B$

and vise versa. In our implementation this is ensured by restricting the set of possible angles to those used to approximate $m(b) \in \mathcal{M}^B$ (see Section 2).

4 On the Dimension of Narrow Passages

Consider the pacman scenario illustrated in Fig. 3c of the experiments section. We obtain a narrow passage by increasing the size of the square-shaped robot making it harder for the pacman to swallow it. Fig. 4 shows that our approach is significantly less sensitive to this tightening than the PRM algorithm. In order to explain this, let us take a closer look at the nature of the narrow passage for the tightest solvable case.

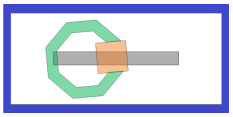

In order to get from the start placement to the goal placement, the pacman must swallow the square, rotate around it and spit it out again. Due to symmetry it is sufficient to concentrate on the first part. The figure to the right depicts the tightest case, i.e., when the square robot fits exactly into the "mouth" of the pacman. The gray rectangle indicates the positions of the reference point of the square such that there is a valid movement of the pacman that will allow it to swallow the square robot (two-dimensional region, two parameters), the rotation angle of the square is also important (one additional parameter). The range of concurrently possible values for all three parameters is small but does not tend to zero. The passage becomes narrow by the fact that the rotation angle of the pacman must correlate exactly with the orientation of the square to allow for passing through the mouth. Moreover, the set of valid placements for the reference point of the pacman while swallowing the square (other parameters being fixed) is a line, i.e., its x and y parameter values are coupled. Thus, the passage is a four-dimensional object as we have a tight coupling of two pairs of parameters in a six-dimensional C-space.

The PRM approach has difficulties to sample in this passage since the measure tends to zero as the size of the square increases. On the other hand, for our approach the passage is only tight with respect to the correlation of the two angles. As soon as the MMS samples an (approximated) volume that fixes the square robot such that the pacman *can* engulf it, the approximation of the volume just needs to include a horizontal slice of a suitable angle and the passage becomes evident in the corresponding Minkowski sum computation.

4.1 Definition of Narrow Passages

Intuition may suggest that narrow passages are tunnel-shaped. However, a one-dimensional tunnel in a high-dimensional C-spaces would correspond to a simultaneous coupling of *all* parameters, which is often not the case. For instance, the discussion of the pacman scenario shows that the passage is narrow but that it is still a four-dimensional volume, which proved to be a considerable advantage for our approach in the experiments. Though, some

sampling based approaches try to take the dimension of a passage into account (e.g. see [9]) it seems that this aspect is not reflected by existing definitions that attempt to capture attributes of the C-space. Definitions such as ϵ-goodness [18] and expansiveness [16] are able to measure the size of a narrow passage better than the clearance [17] of a path, but neither incorporates the dimension of a narrow passage in a very accessible way. As a consequence, we would like to propose a new set of definitions that attempt to simultaneously grasp the tightness and the dimension of a passage.

We start by defining the "ordinary" clearance of a path. The characterization is based on the notion of homotopy classes of paths with respect to a set $\Gamma_{s,t}$, i.e., the set of all paths starting at s and ending at t. For a path $\gamma_0 \in \Gamma_{s,t}$ and its homotopy class $\mathcal{H}(\gamma_0)$ we define the clearance of the class as the largest clearance found among all paths in $\mathcal{H}(\gamma_0)$.

Definition 2. The **clearance** of a homotopy class $\mathcal{H}(\gamma_0)$ for $\gamma_0 \in \Gamma_{s,t}$ is

$$\sup_{\gamma \in \mathcal{H}(\gamma_0)} \{ \sup\{ \rho > 0 \mid B^d_\rho \oplus Im(\gamma) \subseteq \mathcal{C}_{\text{free}} \} \},$$

where $\oplus$ denotes the Minkowski sum of two sets, which is the vector sum of the sets.

By using a d-dimensional ball this definition treats all directions equally, thus considering the passage of $\mathcal{H}(\gamma_0)$ to be a one-dimensional tunnel. We next refine this by definition using a k-dimensional disk, which may be placed in different orientations depending on the position along the path.

Definition 3. For some integer $0 < \boldsymbol{k} \leq d$ the ***k*-clearance** of $\mathcal{H}(\gamma_0)$ is:

$$\sup_{\gamma \in \mathcal{H}(\gamma_0)} \{ \sup\{ \rho > 0 \mid \exists \mathtt{R} : [0,1] \to \mathcal{R} \ \forall t \in [0,1] : \ \gamma(t) \oplus \mathtt{R}(t) B^k_\rho \subseteq \mathcal{C}_{\text{free}} \} \},$$

where $\mathcal{R}$ is the set of d-dimensional rotation matrices and B^k_ρ is the k-dimensional ball of radius ρ. In case the map R is required to be continuous we talk about **continuous *k*-clearance**.

Clearly, the k-clearance of $\mathcal{H}(\gamma_0)$ for $k = d$ is simply the clearance of $\mathcal{H}(\gamma_0)$. For decreasing values of k, the k-clearance of a homotopy class is a monotonic increasing sequence. We next define the dimension of a passage using this sequence, that is, we set the dimension to be the first k for which the clearance becomes *significantly larger*[8] than the original d-dimensional clearance.

Definition 4. A passage for $\mathcal{H}(\gamma_0)$ in $\mathbb{R}^d$ of clearance ρ is called ***k*-dimensional** if k is the largest index such that k-clearance$(\mathcal{H}(\gamma_0)) \gg \rho$. If for every k k-clearance$(\mathcal{H}(\gamma_0)) \not\gg \rho$ then the passage is termed one-dimensional.

[8] We leave this notion informal as it might depend on the problem at hand.

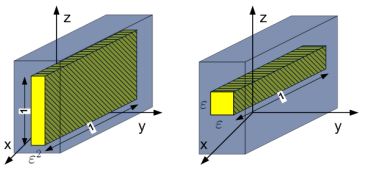

The figure on the right illustrates two three-dimensional C-spaces consisting of a narrow passage (yellow) surrounded by obstacles (blue). Both passages have a measure of ε^2 thus for a PRM like planner, sampling in either passage is equally hard as the probability of a uniform point sample to lie in either one of the narrow passages is proportional to ε^2. However, the two passages are fundamentally different. The passage depicted on the right-hand side is a one-dimensional tunnel corresponding to a tight coupling of the three parameters. The passage depicted on the left-hand side is a two-dimensional flume which is much easier to intersect by a probabilistic approach that uses manifolds as samples. Our new definitions formally reveal this difference. For k equals 3, 2 and 1 the k-clearance of the right passage is ε, $\sqrt{2}\varepsilon$ and larger than 1, respectively. For the left passage this sequence is ε^2 for $k = 3$ and larger than 1 for $k = 2, 1$ which characterizes the passage as two-dimensional.

4.2 Discussion

We believe that the definitions introduced in Section 4.1, can be an essential cornerstone for a formal proof that shows the advantage of manifold samples over point samples in the presents of high-dimensional narrow passages. We sketch the argument briefly. Let $\mathcal{C}_{\text{free}}$ contain a narrow passage of dimension k, that is, the passage has clearance ρ and k-clearance λ, where $\lambda \gg \rho$. This implies that it is possible to place discs of dimension k and radius $\lambda \gg \rho$ into the tight passage. The main argument is that for a random linear manifold of dimension $d - k$ the probability to hit such a disc is proportional to λ, which is much larger than ρ. The probability also depends on the angle between the linear subspace containing the disc and the linear manifold. However, by choosing a proper set of manifold families it should be possible to guarantee the existence of at least one family for which the angle is bounded.

5 Further work

The extension of MMS [29] that is presented here is part of our on-going efforts towards the goal of creating a general scheme for exploring high-dimensional C-spaces that is less sensitive to narrow passages than currently available tools. As discussed in Section 1.3 the original scheme imposes a set of conditions that in combination restrict an application of MMS to rather low dimension. In this paper we chose to relax condition **C3**, namely by computing only approximations of three-dimensional manifolds. An alternative path is to relax condition **C2**, namely by not sampling the manifolds uniformly and independently at random. This would enable the use of manifolds of very low dimension as it allows to enforce intersection among manifolds. Following

this path we envision a single-query planer that explores the C-space in an RRT-like fashion.

Another possibility is to explore other ways to compute approximative manifold samples, for instance, the (so far) exact representations of FSCs could be replaced by much simpler (and thus faster) but conservative[9] approximations. This is certainly applicable to manifold samples of dimension one or two and should also enable manifold samples of higher dimensions. We remark that the use of approximations should not harm the probabilistic completeness as long as it is possible to refine approximations such that they converge to the exact results (equivalent to increased number of samples).

Using these extensions we wish to apply the scheme to a variety of difficult problems including assembly maintainability (part removal for maintenance [37]) employing a single-query variant of the scheme. Additionally, we intend to extend and experiment with the scheme to motion-planning problems for highly-redundant robots as well as for fleets of robots, exploiting the symmetries in the respective C-space.

References

1. Aronov, B., Sharir, M.: On translational motion planning of a convex polyhedron in 3-space. SIAM J. Comput. **26**(6), 1785–1803 (1997)
2. Avnaim, F., Boissonnat, J.D., Faverjon, B.: A practical exact motion planning algorithm for polygonal object amidst polygonal obstacles. In: Proceedings of the Workshop on Geometry and Robotics, pp. 67–86. Springer-Verlag, London, UK (1989)
3. Basu, S., Pollack, R., Roy, M.F.: Algorithms in Real Algebraic Geometry. Algorithms and Computation in Mathematics. Springer-Verlag (2006)
4. Berberich, E., Fogel, E., Halperin, D., Kerber, M., Setter, O.: Arrangements on parametric surfaces II: Concretizations and applications. MCS **4**, 67–91 (2010)
5. Berberich, E., Fogel, E., Halperin, D., Mehlhorn, K., Wein, R.: Arrangements on parametric surfaces I: General framework and infrastructure. MCS **4**, 45–66 (2010)
6. Canny, J.F.: Complexity of Robot Motion Planning (ACM Doctoral Dissertation Award). The MIT Press (1988)
7. Chazelle, B., Edelsbrunner, H., Guibas, L.J., Sharir, M.: A singly exponential stratification scheme for real semi-algebraic varieties and its applications. Theoretical Computer Science **84**(1), 77 – 105 (1991)
8. Choset, H., Burgard, W., Hutchinson, S., Kantor, G., Kavraki, L.E., Lynch, K., Thrun, S.: Principles of Robot Motion: Theory, Algorithms, and Implementation. MIT Press (2005)
9. Dalibard, S., Laumond, J.P.: Linear dimensionality reduction in random motion planning. I. J. Robotic Res. **30**(12), 1461–1476 (2011)
10. De Berg, M., Cheong, O., van Kreveld, M., Overmars, M.: Computational Geometry: Algorithms and Applications. Springer (2008)
11. Foegl, E., Halperin, D., Wein, R.: CGAL Arrangements and their Applications. Springer, Heidelberg (2012)
12. Fogel, E., Halperin, D.: Exact and efficient construction of Minkowski sums of convex polyhedra with applications. CAD **39**(11), 929–940 (2007)

[9] Approximated FSC are contained in $\mathcal{C}_{\text{free}}$.

13. Hachenberger, P.: Exact Minkowksi sums of polyhedra and exact and efficient decomposition of polyhedra into convex pieces. Algorithmica **55**(2), 329–345 (2009)
14. Halperin, D., Sharir, M.: A near-quadratic algorithm for planning the motion of a polygon in a polygonal environment. Disc. Comput. Geom. **16**(2), 121–134 (1996)
15. Hirsch, S., Halperin, D.: Hybrid motion planning: Coordinating two discs moving among polygonal obstacles in the plane. In: WAFR 2002, pp. 225–241
16. Hsu, D., Latombe, J., Motwani, R.: Path planning in expansive configuration spaces. Int. J. Comp. Geo. & App. **4**, 495–512 (1999)
17. Kavraki, L.E., Kolountzakis, M.N., Latombe, J.C.: Analysis of probabilistic roadmaps for path planning. IEEE Trans. Robot. Automat. **14**(1), 166–171 (1998)
18. Kavraki, L.E., Latombe, J.C., Motwani, R., Raghavan, P.: Randomized query processing in robot path planning. Journal of Computer and System Sciences **57**(1), 50–60 (1998)
19. Kavraki, L.E., Svestka, P., Latombe, J.C., Overmars, M.: Probabilistic roadmaps for path planning in high dimensional configuration spaces. IEEE Transactions on Robotics and Automation **12**(4), 566–580 (1996)
20. Kuffner, J.J., Lavalle, S.M.: RRT-Connect: An efficient approach to single-query path planning. In: ICRA, pp. 995–1001 (2000)
21. Ladd, A.M., Kavraki, L.E.: Generalizing the analysis of PRM. In: ICRA, pp. 2120–2125. IEEE Press (2002)
22. Latombe, J.C.: Robot Motion Planning. Kluwer Academic Publishers, Norwell, MA, USA (1991)
23. Lavalle, S.M.: Rapidly-exploring random trees: A new tool for path planning. In Computer Science Dept., Iowa State University **Tech. Rep**, 98–11 (1998)
24. LaValle, S.M.: Planning Algorithms. Cambridge University Press, Cambridge, U.K. (2006)
25. Lien, J.M.: Hybrid motion planning using Minkowski sums. In: RSS 2008
26. Lozano-Perez, T.: Spatial planning: A configuration space approach. MIT AI Memo 605 (1980)
27. Plaku, E., Bekris, K.E., Kavraki, L.E.: OOPS for motion planning: An online open-source programming system. In: ICRA, pp. 3711–3716. IEEE (2007)
28. Reif, J.H.: Complexity of the mover's problem and generalizations. In: FOCS, pp. 421–427. IEEE Computer Society, Washington, DC, USA (1979)
29. Salzman, O., Hemmer, M., Raveh, B., Halperin, D.: Motion planning via manifold samples. In: ESA, pp. 493–505 (2011)
30. Schwartz, J.T., Sharir, M.: On the "piano movers" problem: I. The case of a two-dimensional rigid polygonal body moving amidst polygonal barriers. Commun. Pure appl. Math **35**, 345 – 398 (1983)
31. Schwartz, J.T., Sharir, M.: On the "piano movers" problem: II. General techniques for computing topological properties of real algebraic manifolds. Advances in Applied Mathematics **4**(3), 298 – 351 (1983)
32. Sharir, M.: Algorithmic Motion Planning, Handbook of Discrete and Computational Geometry. 2nd Edition, CRC Press, Inc., Boca Raton, FL, USA (2004)
33. Siek, J.G., Lee, L.Q., Lumsdaine, A.: The Boost Graph Library: User Guide and Reference Manual. Addison-Wesley Professional (2001)
34. The CGAL Project: CGAL User and Reference Manual, 3.7 edn. CGAL Editorial Board (2010). Http //www.cgal.org/
35. Wein, R.: Exact and efficient construction of planar Minkowski sums using the convolution method. In: ESA, pp. 829–840 (2006)
36. Yang, J., Sacks, E.: RRT path planner with 3 DOF local planner. In: ICRA, pp. 145–149 (2006)
37. Zhang, L., Huang, X., Kim, Y.J., Manocha, D.: D-plan: Efficient collision-free path computation for part removal and disassembly. In: Journal of Computer-Aided Design and Applications (2008)

Appendix — Critical Values for Rotating Robot

We consider a polygonal robot rotating about a fixed reference point amidst polygonal obstacles. A critical point is a point representing a configuration of the robot while a feature of the robot is in contact with a feature of an obstacle: Either a robot's edge is in contact with an obstacle's vertex or a robot's vertex is in contact with an obstacle's edge. These cases will be referred to as *vertex-edge* and *edge-vertex* respectively.

The parametrization will yeild a one dimensional line in the configuration space where the FSCs will be intervals along the line. The line will be identified namely the manifold is $\mathbb{RP}^1$. The rest of this section introduces the necessary notions to analyze the problem.

A robot R is a simple polygon with vertices $\{v_1, \ldots, v_n\}$ where $v_i = (x_i, y_i)^T$ and edges $\{(v_1, v_2), \ldots (v_n, v_1)\}$. We assume that the reference point of R is located at the origin. The position of R in the workspace is defined by a configuration $q = (r_q, \theta_q)$ where $r_q = (x_q, y_q)^T$. Thus, q maps the position of a vertex v_i as follows:

$$v_i(q) = M(\theta_q)v_i + r_q, \text{ where } M(\theta) = \begin{bmatrix} \cos\theta & -\sin\theta \\ \sin\theta & \cos\theta \end{bmatrix}$$

is the rotation matrix. Given a fixed point $p = (x_p, y_p)^T$ we define the parametrization $(p, \tau) \in \mathbb{R}^2 \times \mathbb{RP}^1$ in Equation 1

$$x_q = x_p \quad y_q = y_p \quad \theta_q = 2\arctan\tau. \tag{1}$$

The parametrization fixes the robot's reference point, the parametrized vertex is represented in Equation (2)

$$v_i(p, \tau) = M(\tau)v_i + p, \tag{2}$$

where $M(\tau) = \frac{1}{1+\tau^2}\begin{bmatrix} 1-\tau^2 & -2\tau \\ 2\tau & 1-\tau^2 \end{bmatrix}$.

Robot's vertex - Obstacle's edge

Let $r_q = (x_q, y_q)^T$ be the fixed robot's location. Let v_i be a robot's vertex and v_{o_j} where $j \in 1, 2$ be the obstacle's edge's endpoints. The obstacle's edge can be parametrized as $e_o(s) = v_{o1} + s(v_{o2} - v_{o1})$ where $s \in [0, 1]$. If the distance between the fixed reference point and the obstacle's edge is larger than the distance between the robot's vertex and the it's reference point, then the edge cannot impose a constraint. Namely all the edges e such that $d(r_q, e) \geq d(r_q, v_i)$ may be filtered out. A criticality occurs when the robot's vertex coincides with the edge e, thus $e(s) = v_i(r_q, \tau)$ This yeilds the following equalities:

$$x_{o1} + s(x_{o2} - x_{o1}) = \frac{1-\tau^2}{1+\tau^2}x_i - \frac{2\tau y_i}{1+\tau^2} + x_q$$

$$y_{o1} + s(y_{o2} - y_{o1}) = \frac{2\tau}{1+\tau^2}x_i + \frac{1-\tau^2}{1+\tau^2}y_i + y_q$$

Thus:

$$(1+\tau^2)x_{o1} + s(1+\tau^2)(x_{o2} - x_{o1}) = (1-\tau^2)x_i - (2\tau)y_i + x_q(1+\tau^2)$$

$$(1+\tau^2)y_{o1} + s(1+\tau^2)(y_{o2} - y_{o1}) = (2\tau)x_i + (1-\tau^2)y_i + y_q(1+\tau^2)$$

Or,

$$s(1+\tau^2)(x_{o2}-x_{o1})(y_{o2}-y_{o1}) = [(1-\tau^2)x_i-(2\tau)y_i+(1+\tau^2)(x_q-x_{o1})](y_{o2}-y_{o1})$$

$$s(1+\tau^2)(x_{o2}-x_{o1})(y_{o2}-y_{o1}) = [(2\tau)x_i+(1-\tau^2)y_i+(1+\tau^2)(y_q-y_{o1})](x_{o2}-x_{o1})$$

denoting $\Delta_{ox} = x_{o2} - x_{o1}$, and $\Delta_{oy} = y_{o2} - y_{o1}$:

$$[(1-\tau^2)x_i-(2\tau)y_i+(1+\tau^2)(x_q-x_{o1})]\Delta_{oy} = [(2\tau)x_i+(1-\tau^2)y_i+(1+\tau^2)(y_q-y_{o1})]\Delta_{ox}$$

Finally:

$$k_2\tau^2 + k_1\tau + k_0 = 0 \tag{3}$$

Where:
$k_2 = (x_q - x_{o1} - x_i)\Delta_{oy} - (y_q - y_{o1} - y_i)\Delta_{ox}$
$k_1 = -2(y_i\Delta_{oy} + x_i\Delta_{ox})$
$k_0 = (x_q - x_{o1} + x_i)\Delta_{oy} - (y_q - y_{o1} + y_i)\Delta_{ox}$
$\Delta_{ox} = x_{o2} - x_{o1}$,
$\Delta_{oy} = y_{o2} - y_{o1}$

The solutions to Equation 3 are two angles τ_1, τ_2 where $\tau_1 \leq \tau_2$. These parametrized angles represent potential transitions between $\mathcal{C}_{\text{free}}$ and $\mathcal{C}_{\text{forb}}$. These angles may represent intersections that are not on the obstacle's edge but on the line supporting the obstacle's edge. Namely if we obtain s_1, s_2 by pluging τ_1, τ_2 to one of the two following equations and $s_i \notin [0,1]$ then we should not add the corresponding τ_i.

$$s = \frac{(1-\tau^2)x_i - (2\tau)y_i + (1+\tau^2)(x_q - x_{o1})}{(x_{o2} - x_{o1})(1+\tau^2)}$$

$$s = \frac{(2\tau)x_i + (1-\tau^2)y_i + (1+\tau^2)(y_q - y_{o1})}{(y_{o2} - y_{o1})(1+\tau^2)}$$

Robot's edge - Obstacle's vertex

Let $r_q = (x_q, y_q)^T$ be the fixed robot's location. Let v_1, v_2 be the robot's vertex such that the robot's edge is defined as $e(s, r_q, \tau) = v_1(r_q, \tau) + s(v_2(r_q, \tau) - v_1(r_q, \tau))$ for $s \in [0,1]$ and v_o be the obstacle's vertex. If the distance between the fixed reference point and the obstacle's vertex is larger than the distance between the robot's two vertices and the it's reference point, then the vertex

cannot impose a constraint. Namely all the obstacle vertices v_o such that $d(r_q, v_0) \geq d(r_q, v_i)$ may be filtered out. A criticality occurs when a point on the robot's edge coincides with the obstacle's vertex, namely for some $s \in [0,1]$:

$$v_{ox} = v_{1x}(p,\tau) + s(v_{2x}(p,\tau) - v_{1x}(p,\tau))$$

$$v_{oy} = v_{1y}(p,\tau) + s(v_{2y}(p,\tau) - v_{1y}(p,\tau))$$

Thus,

$$(v_{ox} - v_{1x}(p,\tau))(v_{2y}(p,\tau) - v_{1y}(p,\tau)) = (v_{oy} - v_{1y}(p,\tau))(v_{2x}(p,\tau) - v_{1x}(p,\tau))$$

Denoting $\Delta_x = v_{2x} - v_{1x}$ and $\Delta_y = v_{2y} - v_{1y}$:

$$(v_{ox} - v_{1x}(p,\tau))(2\tau\Delta_x + (1-\tau^2)\Delta_y) = (v_{oy} - v_{1y}(p,\tau))((1-\tau^2)\Delta_x - 2\tau\Delta_y)$$

Let us denote $a = (v_{ox} - x_q)$ and $b = (v_{oy} - y_q)$ and $k = v_{1x}v_{2y} - v_{2x}v_{1y}$:

$$[a\Delta_y - b\Delta_x + k]\tau^2 - 2[a\Delta_x + b\Delta_y]\tau + [-a\Delta_y + b\Delta_x + k] = 0$$

$$l_2\tau^2 + l_1\tau + l_0 = 0 \tag{4}$$

Where:

$$l_2 = a\Delta_y - b\Delta_x + k$$
$$l_1 = -2(a\Delta_x + b\Delta_y)$$
$$l_0 = -l_2 + 2k$$

$$\Delta_x = v_{2x} - v_{1x},$$
$$\Delta_y = v_{2y} - v_{1y},$$
$$a = (v_{ox} - x_q),$$
$$b = (v_{oy} - y_q),$$
$$k = v_{1x}v_{2y} - v_{2x}v_{1y}$$

The solutions to Equation 4 are two angles τ_1, τ_2 where $\tau_1 \leq \tau_2$. These parametrized angles represent potential transitions between $\mathcal{C}_{\text{free}}$ and $\mathcal{C}_{\text{forb}}$. These angles may represent intersections that are not on the robot's edge but on the line supporting the edge. Namely if we obtain s_1, s_2 by pluging τ_1, τ_2 to one of the two following equations and $s_i \notin [0,1]$ then we should not add the corresponding τ_i.

$$s = \frac{v_{ox} - v_{1x}(p,\tau)}{v_{2x}(p,\tau) - v_{1x}(p,\tau)}$$

$$s = \frac{v_{oy} - v_{1y}(p,\tau)}{v_{2y}(p,\tau) - v_{1y}(p,\tau)}$$